Heliyon 9 (2023) e22416

Contents lists available at ScienceDirect

Heliyon

journal homepage: www.cell.com/heliyon

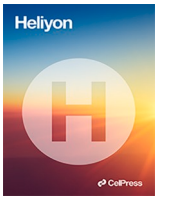

An experimental investigation on the nanofluids in a cavity under natural convection with and without the rotary magnetic field

Debashis Dey [a,b,*], Sukanta K. Dash [a]

[a] Department of Mechanical Engineering, IIT Kharagpur, 721302, West Bengal, India
[b] Department of Mechanical Engineering, Institute of Technical Education & Research (ITER), Siksha 'O' Anusandhan Deemed to be University, Bhubaneswar, 751030, Odisha, India

ARTICLE INFO

Keywords:
Nanofluid
Natural convection cavity
Rotary electromagnetic field
Nanomaterials characterization
Thermo-physical properties

ABSTRACT

This experimental study involves the use of two distinct categories of nanofluids, namely ferro-magnetic and non-magnetic, within a square cavity that facilitates natural convection. There are five distinct concentrations associated with each nanofluid. Natural convection arises as a consequence of the thermal gradient between the opposing surfaces of the copper cavity, which has a thickness of 18 gauge. The purpose of utilizing the constructed electro-magnet assembly is to investigate the impact of the rotational magnetic field on the process of heat transfer. The manipulation of magnetic strength can be achieved by regulating the magnetic power and direct current (DC) power. The manipulation of the electromagnet's spin can also be regulated. In the context of a rotational magnetic field, it is seen that the magnetic flux undergoes a transition from a positive value to an almost identical negative value throughout a full rotation. The optimal heat transfer performance is observed at a nanoparticle concentration of 0.1% by volume (φ) for both nanofluids. In the absence of a rotating magnetic field, the ferromagnetic nanofluid exhibited superior performance. When the Rayleigh number (Ra) is one order smaller than the critical Rayleigh number value, the heat transfer performance is often superior with nanofluid compared to demineralized water.

1. Introduction

The investigation of natural convection within a cavity has been ongoing for almost fifty years. The utilization of nanofluid in a natural convection cavity has been seen for twenty years. The topic of nanofluid research has been divided into four distinct sub-areas by S.R. Babu et al. [1] over the past two decades. The sub-field of free convection in nanofluids is comparatively underexplored in academic research. There has been a significant increase in nanofluid research over the past two decades, characterized by exponential expansion. Sivaraj and Banerjee [2] have characterized nanofluid research in convective cavities as encompassing the study of nanofluid flow in many cavity shapes and sizes, including cavities with barriers, normal enclosures, and wavy enclosures, among others.

The majority of experimental investigations on natural convection utilizing nanofluids have been conducted within a square enclosure, with the most favorable nanoparticle concentration observed at low values of φ, and within the range of $10^6 < Ra < 10^9$. In a study conducted by Garbadeen et al. [3], it was observed that the highest level of heat transmission, with a significant increase of 45%,

* Corresponding author. Department of Mechanical Engineering, IIT Kharagpur, 721302, West Bengal, India.
E-mail address: debashisdey@soa.ac.in (D. Dey).

https://doi.org/10.1016/j.heliyon.2023.e22416
Received 16 March 2023; Received in revised form 9 October 2023; Accepted 11 November 2023
Available online 14 November 2023

was observed at a φ of 0.1%. The identical optimal concentration is identified by Ho et al. [4], Shariful et al. [5], Ghodsinezhad et al. [6], and other researchers. The effective thermal conductivity (K_{eff}) of nanofluids is higher than that of the base fluid, leading to an improvement in heat transmission. Nevertheless, Rahimi and colleagues [7] discovered that the optimal value for φ is 0.05%. Despite the increase in concentration, the temperature distribution within the core region remains unchanged. According to the findings of Heris et al. [8], the maximum enhancement in heat transfer occurs when the concentration of titania particles (TiO_2) is low and the inclination angle is set at 90°. The increase in Nusselt number (Nu) for nanofluids is comparatively lower than that of turbine oil, mostly attributed to the phenomenon of aggregation.

The stability of nanofluids within cavities undergoing natural convection is a significant difficulty. Various methods have been employed by researchers to promote stability, including functionalization, pH modification, and the application of electric fields. Ilyas and colleagues [9] have employed carboxylic acid functionalization of the nanoparticles to enhance their stability. The degradation of Nu, which represents the Nusselt number, is observed as the concentration increases, primarily due to the corresponding increase in μ_{eff} (effective dynamic viscosity) and ρ_{eff} (effective density). In a study conducted by Kouloulias et al. [10], it was demonstrated that the absence of a pH change or surface activator leads to a decrease in heat transfer performance, accompanied by a weakening of the electrostatic repulsion force. The absence of fluid motion and the presence of agitation are additional factors contributing to this phenomenon. According to Chen et al. [11], the presence of an electrical field has a beneficial impact on the process of heat transfer. Specifically, when there is frequent switching, the heat transfer becomes more noticeable.

According to Hu et al. [12], the temperature difference is identified as the predominant factor influencing the distribution of nanoparticles, and this effect is observed to intensify with increasing Rayleigh number (Ra). Khalili and colleagues [13] have observed the existence of non-uniform φ beyond the second or fourth levels of the walls. The value of φ near the cold border is greater than that near the hot wall for all Ra values. Various physical phenomena, such as Brownian motion, convection, thermophoresis, and gravity, contribute to this phenomenon. The researchers Hu et al. [14] have noted that when the Rayleigh number (Ra) is low, the nanofluid exhibits a greater sensitivity to variations in the effective viscosity (μ_{eff}) compared to the effective thermal conductivity (K_{eff}). According to the findings of Solomon et al. [15], an increase in the aspect ratio (AR) leads to a rise in the ideal φ required for achieving maximum heat transmission. As the aspect ratio (AR) falls, there is an observed rise in charge quantity and cavity size, accompanied by enhanced fluid circulation resulting from increased buoyancy. This improved fluid circulation subsequently leads to enhanced heat transfer. According to the findings of Malekshah and Salari [16], it has been observed that the value of Nu_{avg} decreases as the aspect ratio (AR) increases. As the ratio increases, the temperature of the entire water region increases due to a decrease in the amount of water contained within the enclosure. The convective flow driven by natural convection exhibits a notably low intensity in the lower region of the cavity. According to the findings of Haddad et al. [17], a decrease in APS (average particle size) from 250 nm to 5 nm leads to an increase in heat transfer. Brownian motion enhances convective heat transfer. The worsening of heat transmission, as indicated by the average Nusselt number (Nu_{avg}), is reduced at decreasing aspect ratios (AR) of the cavity. The μ_{eff} models exhibit more sensitivity compared to the K_{eff} models. The increase in heater length leads to a decrease in average heat transfer for a modest inclination angle. However, the effect of heat transfer enhancement is negligible at low Rayleigh numbers. At a specific Rayleigh number, the rate of heat transfer exhibits a decrease as the value of φ increases. For all values of Ra, there is a degradation in systematic heat transfer when φ is equal to or greater than 2%.

Different slip mechanisms in the natural convection cavity are explained in detail in references [18,19]. Brownian diffusion is one such slip mechanism that refers to the phenomenon of nanoparticles undergoing rapid and stochastic movement. Thermophoresis refers to the phenomenon in which the movement of nanoparticles is induced by a temperature gradient present in the surrounding base fluid. The Magnus effect arises from the presence of a velocity gradient, causing particles to rotate along an axis that is perpendicular to the axial flow. Fluid drainage occurs as a result of the pressure gradient, leading to the formation of a thin liquid drainage layer close to the wall. Diffusiophoresis refers to the phenomenon wherein nanoparticles are propelled by the concentration gradient present in the surrounding base fluid. Additionally, the nanoparticles undergo gravitational settling. In a study conducted by Bahiraei [20], it was demonstrated that in addition to the previously indicated mechanisms, namely Saffman lift force, Soret and Dufour effects, and non-uniform shear rate viscosity gradient, particle migration can also be attributed to these factors. Particles tend to migrate from regions of high shear to regions of low shear.

According to Prasher [21], the transfer of thermal energy in nanofluids can be attributed to various factors, including translational Brownian motion, inter-particle potential (associated with phonon-like energy modes), and convection in the liquid resulting from Brownian movement. Among the several components considered, the last factor is accountable for augmenting the thermal conductivity enhancement factor of nanofluids. According to the findings of Jang and Choi [22], the phenomenon of heat transfer increase in nanofluids can be attributed to four distinct modes. The phenomena observed in this system include the interactions resulting from collisions between the molecules of the base fluid, the process of thermal diffusion occurring among the suspended nanoparticles, the collisions between nanoparticles resulting from their Brownian motion, and the thermal interactions between the nanoparticles and the molecules of the base fluid.

In their study, Dey and Sahu [23] conducted experimental observations of circulation by employing smoke and color dye experiments in air and water mediums respectively. The flow of circulation occurs from the region with a higher temperature to the region with a lower temperature within the cavity. The authors, Corvaro and Paroncini [24], conducted a study on the visualization of natural convection flow in the air using a non-intrusive technique known as 2D-PIV (particle image velocimetry). In this study, the examination of velocity vectors and the occurrence of vortex flow separation is conducted for varying placements of the heat source within the cavity. The symmetrical arrangement has been seen to exhibit the highest velocity and is considered optimal for natural convection. The Mach-Zehnder Interferometer (MZI) is employed in experimental settings, and its findings are juxtaposed with the numerical outcomes presented by Kumar et al. [25]. Increased density and enhanced uniformity of fringe patterns correspond to elevated

levels of heat transfer. It has been noted that near the heat source, there is a high Rayleigh number (Ra), and significant natural convection occurs for substantial openings, resulting in increased heat transfer and flow rate. Rao and Srivastava [26] have employed the Mach-Zehnder interferometer (MZI) technique to investigate Rayleigh-Benard (RB) convection inside a three-dimensional temperature distribution. The reconstruction process employs the iterative multiplicative algebra reconstruction technique, commonly referred to as MART. Within this particular domain, the terms "peaks" and "valleys" are used to denote the phenomenon of solid convective motion. The temperature spectra known as Bolgiano-Oboukov are observed in water according to the 7/5th law, while the temperature spectra referred to as Kolmogorov are noticed in mercury based on the 5/3rd rule [6]. Dixit and Pattamatta [27] conducted an experimental investigation within a cubical acrylic cavity, focusing on the range of $10^6 < Ra < 10^7$ and utilizing a homogeneous magnetic field of 0.13 T (Tesla). The heat transmission efficiency of MWCNT (multi-walled carbon nano tube), graphene, and Cu (copper) is diminished, while the silica nanofluid remains unaffected. The force experienced by a charged particle due to the presence of a magnetic field, as described by Lorentz's force law, is directly proportional to the square of the magnitude of the magnetic field. Therefore, as the magnetic field strength increases, the velocity component experiences deceleration, resulting in a decline in convection heat transfer efficiency.

In their study, Leong et al. [28] have put forth three correlations to determine the Nusselt number concerning the direction of an air-filled cubical cavity. Similarly, Cioni et al. [29] have presented a connection specifically for RB convection. The experimental investigation of a rectangular enclosure containing a sub-micron polystyrene-water suspension has revealed that the reduction in heat transfer can be attributed to the phenomena of Brownian motion and thermophoresis. Putra et al. [30] have identified a consistent and conclusive decline in heat transmission. The degradation seen is more pronounced in the case of CuO (copper oxide) compared to Al_2O_3 (alumina), and the heat transfer by natural convection is lower than that of pure water. The significance of particle-fluid slip and sedimentation in this context cannot be overstated. Li and Peterson [31] also observed a decline in natural convection heat transfer. A systematic decrease in heat transmission has been seen when φ increases. The decrease in effectiveness can be attributed to the increased effective mobility as well as the enhanced Brownian and thermophoretic motion shown by the nanoparticles. The frequency of the Tollmien-Schlichting type instability (2 Hz) has been seen in the turbulent boundary layer of an isothermal vertical wall located within a natural convection cavity, as reported by Weppe et al. [32]. This observation aligns with the principles of linear stability theory as applied to a vertical hot plate.

There have been a few experiments done with nanofluids in the natural convection cavity. For the natural convection chamber, the rotating electromagnetic field has not been used yet. In this study, we looked at ferromagnetic and non-magnetic nanoparticles in the natural convection cavity with and without a rotating electromagnetic field. The nanomaterials have been described, and the qualities of nanofluids have been measured. Then, both types of nanofluids are compared, and the best amounts are found.

2. Experimental set-up

The experimental configuration for natural convection within a cavity comprises several mechanical, electrical, and electronic components. Fig. 1 displays the experimental set-up, revealing the primary components. All of these components are interconnected by means of pipework, wires, or screws. The cavities, constant-temperature water baths, pipes, and other components are effectively insulated to prevent any thermal energy dissipation. The cavity is positioned at an elevated level to accommodate the installation of a rotational electromagnetic assembly beneath it. The utilization of this assembly facilitates the generation of a rotational magnetic field, hence becoming advantageous for conducting flow visualization studies. Simultaneous tilting of both the cavity and the electromagnetic assembly is possible. The major parts of the experimental set-up are a rotary electromagnet, a spiral winding heater inside the glass-wool at the heating side of the cavity, and a refrigeration unit with the condenser, compressor, fan, heat exchangers, etc.

It has the following parts: e.g., square natural convection cavity (at the top), rotary magnetic field (below the cavity), and control

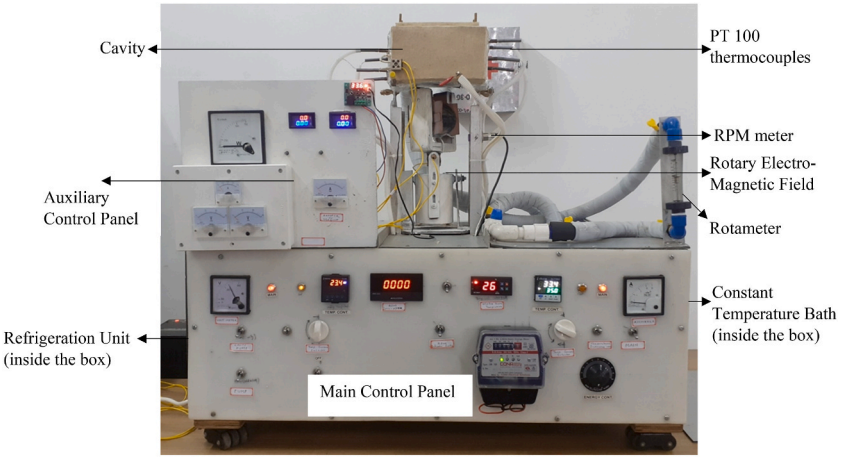

Fig. 1. Natural convection cavity experimental set-up [33].

panels (two numbers, i.e., main and auxiliary, on the front side), constant temperature water bath (right side of the box below), rheostat (type 2P1, for controlling the heater power), and refrigeration unit (left side of the box below). The main control panel has an analog voltmeter, an analog ammeter, four signal indicators, eight toggle switches, two selector switches, two temperature controllers, a rpm indicator, a water bath temperature digital display, an energy controller, an energy meter, etc. The auxiliary control panel mounts an analog wattmeter, the digital display of the bulk temperature of the cavity fluid, an analog ammeter, and a voltmeter each for both the electro-magnet and the DC motor, etc. The rotary magnetic field consists of a wound copper coil (24 gauges) all around the 'U'-shaped iron and DC powered.

This coil assembly's rotation and magnetic strength can be controlled externally. The heat is taken out of the square natural convection cavity using a cooling water jacket. This is connected to the constant water temperature in the bath. The temperature of the bath is set by the user. The refrigeration unit cools down the bath using a counter-flow heat exchanger. Refrigerant (R134a) rejects the same heat into the atmosphere via a condenser. The temperature difference between the hot and cold sides is kept within 10 °C so that the bulk fluid properties can be assumed to be constant. A rotameter is used to measure the flow rate from the bath to the cavity. It can vary between 0 and 6 LPM (litres per minute). The RPM (revolutions per minute) meter measures the rotary speed of the electromagnet assembly. The typical rpm value is kept between 50 and 75 rpm. Eight PT 100 thermocouples are mounted on the hot and cold sides of the cavity to measure the temperatures and are displayed by iTherm temperature controllers (Model Nos. NX 441 and AI 7482). The resolution of these temperature controllers is 0.1 °C. There is also a provision for temperature settings for both controllers.

A square cross-section (10 cm × 10 cm) cavity of 20 cm length is used in this investigation. This cavity is filled with a 2-L nanofluid. The top of the cavity can be opened to pour the liquid into the cavity. The constant temperature of the hot side is maintained by making an intermittent heat supply using a spiral winding heater on the left copper wall (from the bath side) of the cavity. The heater will start when the temperature drops below the set value and vice versa. The isothermal cold copper wall is maintained using a water jacket, and it is connected to a fabricated constant-temperature water bath. A 1 kVA BPE-supplied UPS is also used to avoid any sudden shutdown of the system due to a power outage.

The DC passes through the two spring-held carbon bushes to the copper-plated vertical stepped shaft of the electromagnet assembly. There is a separate power connection to the DC motor as well. Both electromagnet and DC motor input voltages and currents are monitored by the analog CALANDIS 85C1 DC voltmeter (0–30 V) and the XOXOX DC ammeter (0 – 2 A). The electromagnet is created by winding the copper wire over the mild steel block. The electromagnet part is kept inside the U-shaped wooden blocks to

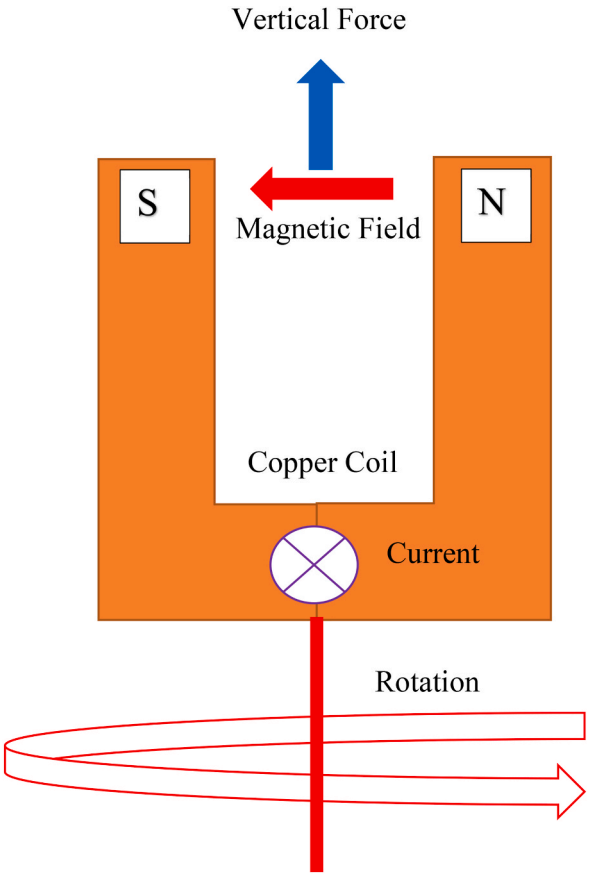

Fig. 2. Rotary electromagnetic field, current, and force directions.

protect its magnetic flux. The whole electromagnetic assembly is kept below the cavity. There are ceramic beads all along the spirally wound heater. The heating side wall is filled with glass wool after placing this heater. This heater is connected to the rheostat. It can control the heater's input power. Heating side power is measured by an analog wattmeter (maker: Eletech, 0–750 W). The rotating magnetic field with current, force, rotation direction, and copper coil position are shown in Fig. 2.

Each vertical side wall has four PT100 temperature sensors. These are connected to the temperature controllers. The average of all four temperature sensor readings is the heating side (T_H) and cooling side (T_C) temperatures, respectively, as shown in equations (1) and (2).

$$T_H = \frac{T_1 + T_2 + T_3 + T_4}{4} \tag{1}$$

$$T_C = \frac{T_5 + T_6 + T_7 + T_8}{4} \tag{2}$$

$$\text{The heatremovedusing the cooling jacket, } Q_c\ (\text{W}) = \rho V C_p\ (\Delta T) \tag{3}$$

$$\text{Heat transfer coefficient}\left(\text{h, W} \,/\, \text{m}^2\text{–K}\right) = \frac{Q_C}{A \times (T_H - T_C)} \tag{4}$$

$$\text{Nusselt number from the experiment, } Nu = \frac{hH}{K_f} \tag{5}$$

The specific heat capacity (C_p) and thermal conductivity (K_f) of the fluid are at T_9 (°C), i.e., the bulk temperature of the fluid inside the natural convection cavity. The Rayleigh number (Ra_H) is also calculated using the fluid properties at the bulk temperature. Both Nu and Ra_H are the averages of the three readings. In equation (3), ΔT is the temperature gained by the flowing water after passing through the cooling jacket. This value is typically between 0.1 °C and 0.3 °C. The temperature gained by the flowing water remains almost constant for a particular concentration and bulk temperature. However, with the increase in heat flux and magnetic field introduction, this gain varies. The volumetric flow rate is 6 L/min between the constant-temperature water bath and the cooling jacket. All the major instruments used in this investigation are summarized in Table 1 below with their accuracies.

The area (A) under consideration for equation (4) is 0.02 m^2. The height (H) of the cavity is 0.1 m for equation (5). As the bulk temperature of the cavity increases, the temperature difference between the two sides also increases at equilibrium. The cold side temperature remains almost the same as measured by four PT100 sensors. However, the hot side temperature fluctuates between 2 °C and 4 °C at equilibrium. Because it has constant heat flux boundary conditions. The time required for one cycle of fluctuation in temperature increases with the increase in nanoparticle concentration. A temperature is set on the AI7482 controller. If the temperature goes 0.2 °C below this set value, then the heater will be ON. As soon as the temperature reaches the set value, the heater will be OFF. This variation in temperature makes the hot side temperature fluctuate with a mean equilibrium. This fluctuation rate will be slower at higher temperatures. Similarly, when the temperature of the cold bath increases by 1 °C, the compressor of the refrigeration unit will be ON. The extra heat from the bath will be removed, and again, it will be back to the set temperature. The resolution of this digital Nagman 201 platinum-type resistance thermometer is 0.01 °C. It can store in its memory up to 99 readings. The piercing probe (PT-100, IEX751, class A) has to be inserted into the water 15 times its diameter (5 mm) from the probe tip to get the correct temperature. The temperature sensor length is 230 mm. It can also take note of the relative reading so that we can directly get the difference in temperatures. It has a sampling rate of two times per second. This meter uses a 9 V alkaline battery with 100 h of life.

The digital Gauss meter in Fig. 3 is used to measure the magnetic intensity of the fabricated rotary electromagnetic field. As the DC power decreases, so does the magnetic flux (Gauss) of the electromagnet. The poles of electromagnetics are identified by the compass. The electromagnet is connected to a DC voltmeter and ammeter for voltage and current measurements to get the power requirements of the electromagnet. The one flat side of the TE-111 probe measures positive gauss on one pole and negative gauss on the other pole. The range of this meter is selected as 2000 (2 K). So, the values we get from the machine will be multiplied by 2000 to get the actual magnetic flux.

The hysteresis curve in Fig. 3 can be used for calibration purposes for both upward and downward DC power values and the corresponding magnetic flux values. The relationship between these two parameters is not linear but rather a second-order polynomial fit. The zone between the two curves creates the hysteresis loop. The second-order polynomial fit equations and R^2 values are also

Table 1
Instrument lists and their accuracies.

Serial No	Instrument Name	Accuracy
1	RTD (Resistance Temperature Detector) Thermometer	0.01 °C
2	Temperature/EC/TDS meter	0.1 °C
3	pH meter	0.1
4	Digital flux/Gauss meter	0.001 G
5	KD2 Pro	0.001 W/m °C
6	Brookfield Viscometer	0.01 cP
7	MDSC(Modulated Differential Scanning Calorimeter)	0.001 J/g °C

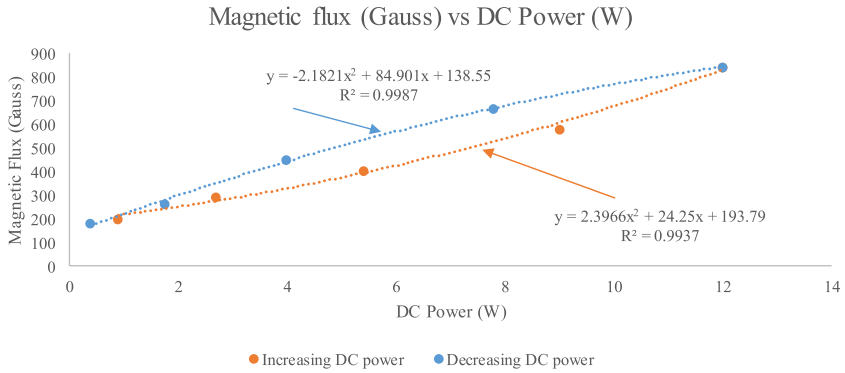

Fig. 3. Hysteresis curve of the rotary-electromagnet.

shown in this figure. If the electromagnet rotates, then the magnetic flux fluctuates between a positive and negative value. The value reaches its maximum when the current passes through the electromagnet, as indicated by the DC ammeter. With the power increase, the magnetic flux value improves, but it is independent of the rpm of the electromagnet.

As it is a rotating magnetic field, the intensity also varies. The tip of the probe is kept between the cavity and the rotary electromagnet. The fluctuating magnetic intensity is noted down (both the minimum and maximum values) for each rpm at various magnetic strengths. The rotary magnetic field can rotate the 1.5-inch magnetic bead clockwise (from the top) for all mediums (air, demineralized water, and transformer oil). However, ferromagnetic iron oxide nanoparticles do not move at all in the transformer oil. The dynamic viscosity of this oil is approximately fourteen times greater than that of demineralized water. This viscous resistance force is higher than the external rotary magnetic force. Thus, these nanoparticles cannot move. But in the air and the demineralized water, the inner iron oxide nanoparticles (group) rotate around their axes and also revolve around the centre of the rotary electromagnetic field. The outer nanoparticles move like amebae and also revolve around the centre of the rotary electromagnetic field, according to Dey et al. [33]. Gradually, all the nanoparticles reach the centre of the rotary magnetic field.

3. Nanomaterials characterization

Two types of nanoparticles are used in the natural convection cavity. Both the nanoparticles are purchased from Sigma-Aldrich, Hyderabad. The γ-alumina (Al_2O_3) nanoparticle APS is 13 nm and the iron oxide nanoparticle APS is between 50 nm and 100 nm. These particles are suspended in the base fluid demineralized (DM) water and then either ultra-sonication (at 40 kHz) or magnetic stirring is done for 2 h. The properties like temperature, electrical conductivity, total dissolved solids, and pH of nanofluid solutions are measured using the TDS (total dissolved solids) meter and pH meter, respectively.

The SEM (scanning electron microscopy) machine is integrated with EDS (energy dispersive spectroscopy) and color mapping. There was a gold vapor cover (pink color) over the samples by sputtering using the machine in Fig. 4. The EDS image has predominant peaks of only iron (Fe) and oxygen (O). The weight percentage of Fe is 67.9% and that of O is 32.1%, as per eZAF quantity results. So, no other element or peak related to the impurity is present in this analysis.

The color mapping (Fig. 5) shows the uniform presence of both atoms (cyan color for iron and purple color for oxygen) in the sample. XRD (x-ray diffraction) is used for both nanoparticles (crystallite samples). One of the most important uses of XRD is phase

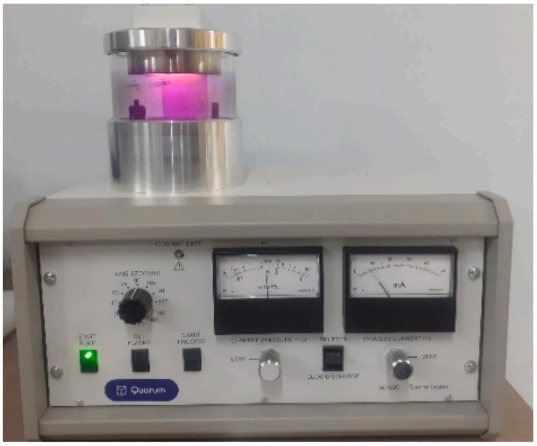

Fig. 4. Au–Pd (Gold–Palladium) plating on the SEM samples at CNSNT, ITER Laboratory.

identification. The orientation of the planes of highly packed atoms is similar to those reported in the standards. XRD of iron oxide (II, III) nanoparticles and γ-Al_2O_3 nanoparticles and comparison with references are shown by Dey et al. [33].

4. Nanofluid properties

The nanofluid is prepared by a two-step method as shown in the flow chart of Fig. 6.

All the thermal conductivity and dynamic viscosity properties of nanofluids are measured at VIT, Vellore. KD-2 Pro is used for thermal conductivity measurement, and the Brookfield viscometer is used for the dynamic viscosity of the nanofluids. Each reading is taken at least twice after ultra sonication. In total, ten different nanofluid samples were tested at five different temperatures. The color of ten nanofluid samples is shown in the test tubes in Fig. 7. There is a gradual increase in color intensity with the nanoparticle concentrations. After 2 h of magnetic stirring or ultra sonication, these solutions remain stable for a minimum of one day. The same concentration of nanofluids is used in the natural convection cavity as well. The nanofluid properties are mentioned in detail by Dey et al. [33,34].

4.1. Dynamic viscosity of the nanofluids

The Brookfield viscometer used the spindle number 18, 80 rpm, and a single point for 30 s. The temperature of the sample varies between 30 °C and 80 °C. Based on the readings of two samples (out of ten), the following plots are generated for the viscosity over the temperature range. The dynamic viscosity of alumina nanofluid varies linearly with temperature, and iron oxide nanofluid variation is a power law type. There is a decrease in viscosity for both nanofluids with temperature. However, this decrease is less for iron oxide nanofluids, as shown in Fig. 8b.

4.2. Thermal conductivity of the nanofluids

Thermal conductivity of alumina and iron oxide nanofluids of five different concentrations between 30 °C and 70 °C are measured by KD2 Pro from VIT (Vellore Institute of Technology), Vellore Laboratory.

Two different nanofluid concentrations (four to five values) are curve-fitted using Excel, as shown in Fig. 9. It is found that the variation over this temperature range at low concentrations is linear, but it becomes non-linear at the highest concentration for both nanofluids. There is only one exception for the 0.05% by volume iron oxide (II, III) nanofluid case. This solution may not be well

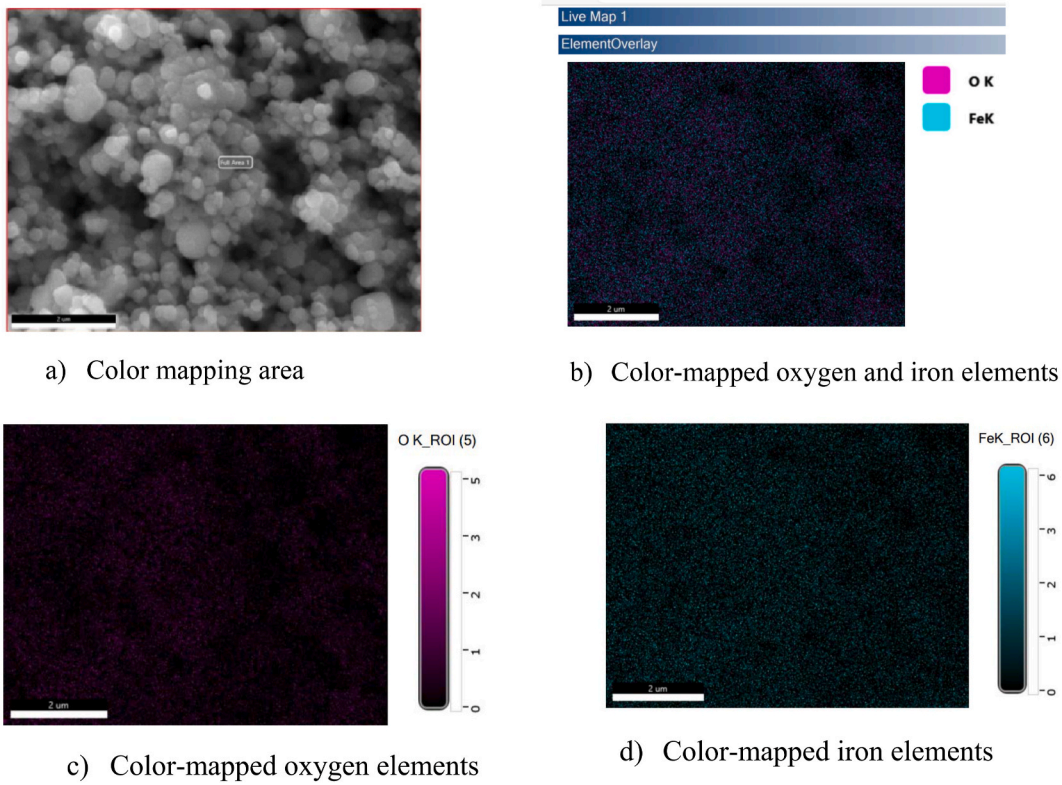

Fig. 5. Color mapping of iron oxide elements.

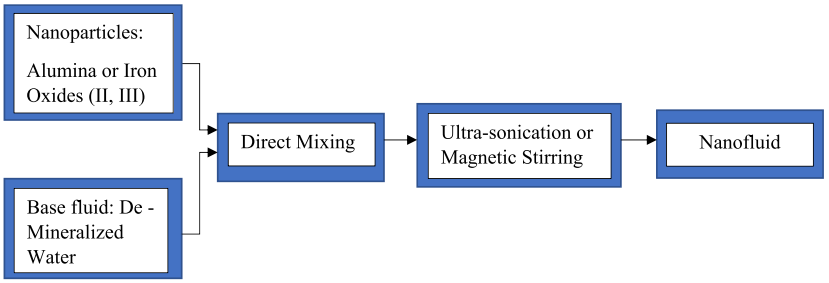

Fig. 6. Nanofluid preparation by a two-step method.

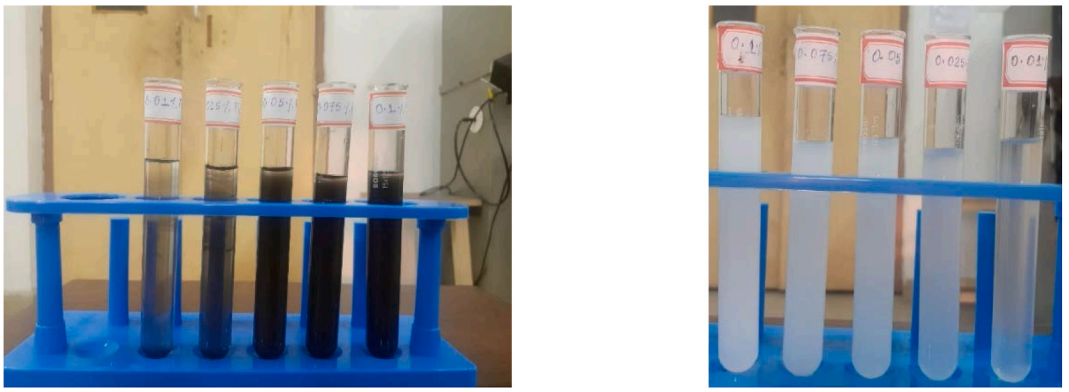

Fig. 7. Five iron oxides and five alumina nanofluid solutions of varying concentrations.

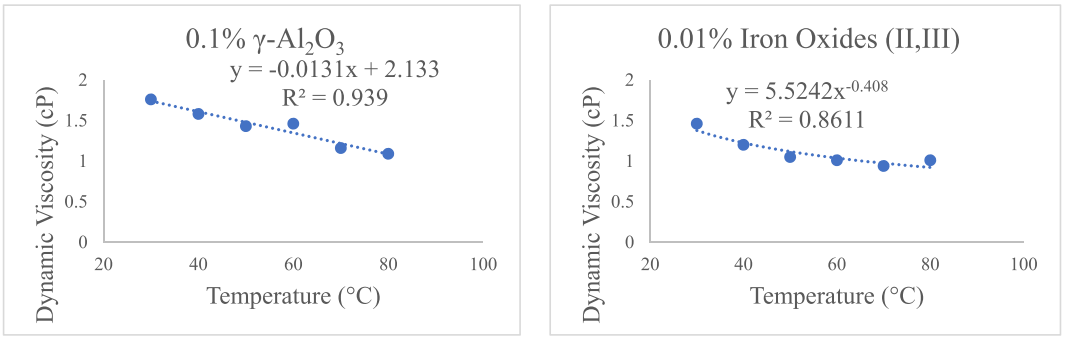

Fig. 8. Dynamic viscosity plot of γ-Al_2O_3 and iron oxides (II, III) solutions with temperature.

stirred, or stability may be an issue before measuring the thermal conductivity using KD-2 Pro at VIT, Vellore. These values are used to calculate the Nusselt numbers at the cold wall of the cavity using equation (7). The higher this thermo-physical property is, the more conduction there will be through the nanofluid. In a natural convection cavity, the convection current will become less if conduction heat transfer is too high, i.e., particles will be stagnant, and particle-to-fluid or vice versa, particle-to-particle conduction heat transfer will take place in such a case.

5. Results and discussion

All the following plots were generated using Matlab R2016b. In these cases, the concentration of nanoparticles is increased to find an optimum solution for the natural convection cavity under a rotary magnetic field and without it.

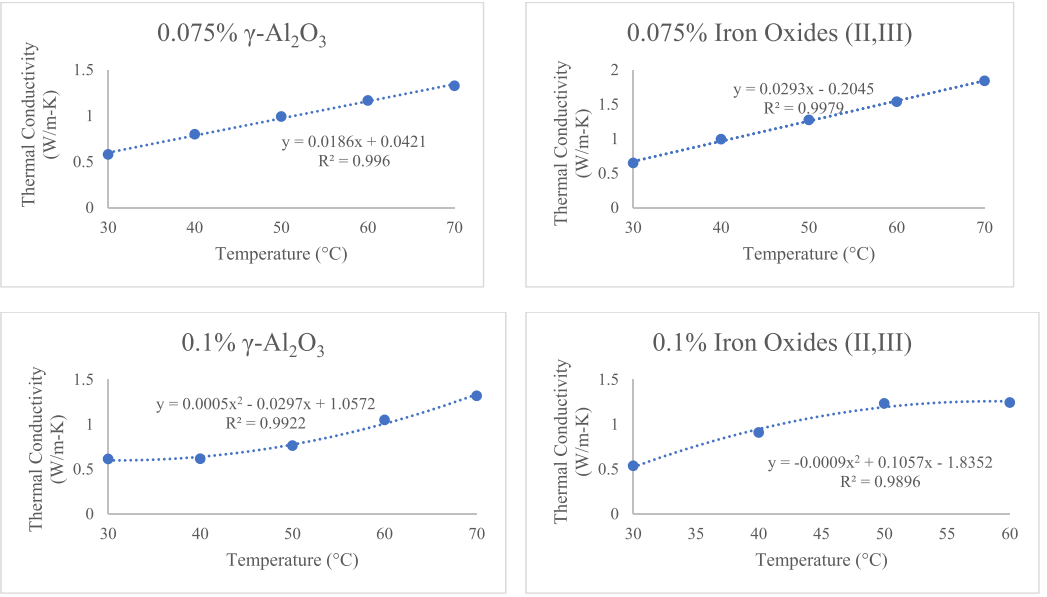

Fig. 9. The variation of thermal conductivity of nanofluids with temperatures.

5.1. γ-Alumina nanofluid in natural convection cavity

The benchmark lines (blue and magenta) are shown in Fig. 10 for pure water. The following two equations (6) and (7) are considered from the benchmark papers:

$$\text{Cioni et al.}(1996), \text{Nusselt number:} Nu = 0.185 Ra_H^{0.292} \tag{6}$$

$$\text{Leong et al.}(1999), \text{Nusselt number:} Nu = 0.08461 Ra_H^{0.3125} \tag{7}$$

Validation testing shows that green stars are lying between these two lines. If nanofluid is used, then in most Rayleigh numbers (Ra_H), there is an improvement in Nusselt number values.

In addition, if the rotary magnetic field is implemented, there is higher heat transfer at high Ra_H values. In the case of γ-alumina nanofluid, a 1.5-inch magnetic bead is kept inside the cavity. Apart from the magnetic field effect on the nanofluid, a magnetic bead creates agitation so that nanoparticles do not settle at the bottom of the cavity. Thus, the magnetic field affects both the nanofluid and the magnetic bead for nanofluid stability enhancement. If the rpm of the rotary magnetic field is improved, then agitation will be greater, but the carbon bush will erode faster. The spring-loaded two carbon bushes supply the power to the rotary magnetic field. So, the typical range for this rotation of the electromagnet is kept between 50 and 75 rpm. The power requirement for both the magnet coil

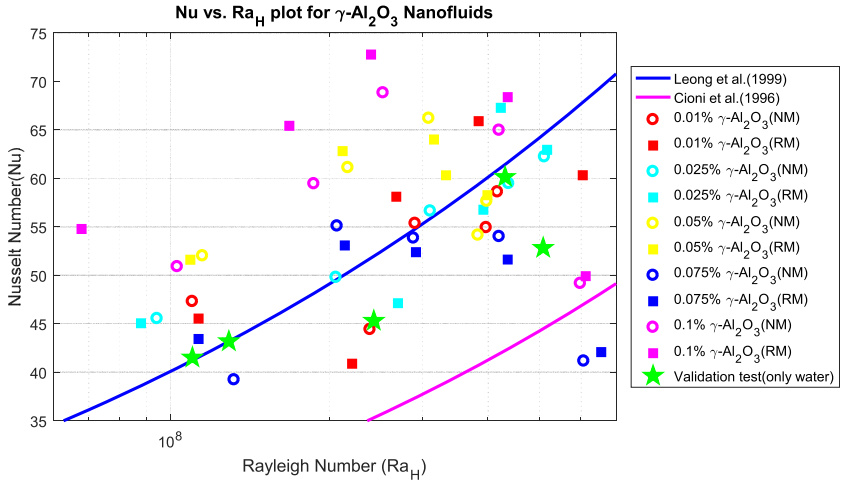

Fig. 10. Nusselt number vs. Rayleigh number plot for γ-Al_2O_3 nanofluids.

and the motor is also very low (between 4 W and 12 W).

However, at low RaH values, there is no improvement in heat transfer. There are many points higher than the upper blue line, which suggests that there is a possibility of improvement in Nu values using nanofluid at a higher RaH value. This improvement can happen with or without a rotary magnetic field. Each steady-state data point is taken three times, and then the average values are considered. The repeatability of the data is found in all readings that are used for plotting. The typical time to reach a steady state is approximately 2 h.

If the concentration of the nanoparticle increases, then higher RaH values are a good choice for better convective heat transfer. This can be achieved at a higher temperature of the hot surface or at a higher temperature of the bulk fluid in the cavity. In this case, the magnetic field works well over the nanofluid, as shown in Fig. 10. It is clear that even if the magnetic field is not applied, nanofluid can help transfer more heat. However, after a long duration, most of the nanoparticles settle at the bottom of the cavity. This is more so because there is no bulk motion in this static fluid. So, intermittent agitation using an external force field can help this non-magnetic particle achieve better stability. Otherwise, manual agitation using a stirring rod will be needed after certain time intervals.

If we keep on increasing the nanoparticle concentration, then there are more outliers (not in between the benchmark lines) where Nu will be higher than in the previous cases. So, we can observe a positive trend here with nanoparticle concentration, rotary magnetic field effect, and heat transfer. However, this result is not true for the whole range of Ra_H values considered in these experiments. But nanofluid with or without a rotary magnetic field always has a better Nu value than the base fluid in water-only cases. Higher Ra_H values mean more turbulence in the solution. The vortex movement from the hot wall to the cold wall will also be faster. So, it takes less time to reach a steady state and transfer the heat from the hot wall to the cold wall and from the cold wall to the constant-temperature bath. This heat will ultimately be released into the atmosphere using a vapor compression refrigeration unit. This intermittently mixed-mode convection will be a better choice near the critical Ra_H values (laminar to the turbulent transition). As we keep on increasing the nanoparticle concentration, there are very few outliers at 0.075% concentration. The rotary magnetic effect has less effect on convective heat transfer. At a high Rayleigh number (near the critical value), there are detrimental Nusselt number values for both cases. In this case, almost every data point lies between the two benchmark correlations (blue and purple lines). In general, nanofluid performs better than the base fluid, water (validation test).

At a concentration of 0.1%, nanofluid performs much better than the base fluid, water. However, at a very high Rayleigh number, there is deterioration in the Nusselt number. Because at high cavity temperatures, it is difficult to maintain the small temperature difference ($<10\ ^\circ C$). The rotary magnetic field is enhancing convective heat transfer. Even if the particle is non-magnetic, there is still a positive effect on heat transfer. The agitation created by the magnetic bead may be responsible for this. Almost every data point is an outlier in this case.

If we observe all ten cases with five data points for each alumina nanofluid, then there will be a maxima in general. However, the improvement in heat transfer from non-magnetic to rotary magnetic is observed at 0.1% concentration for all five data points. So, at lower nanoparticle concentrations, the rotary magnetic effect has not helped in improving the Nu values at all. If Ra is too high (very close to the critical value), then due to the instability, Nu deteriorates.

5.2. Iron oxide (II, III) nanofluid in natural convection cavity

At low Rayleigh numbers, Nu is improved for both rotary and non-rotary magnetic field cases. This improvement is marginally greater under the rotary magnetic field effect, as shown in Fig. 11. The nanoparticles are heat carriers from the hot wall to the cold wall through the bulk fluid. In the major region of the cavity, bulk fluid heat transfer is by conduction only. So, the motions of the particles under the influence of the rotary magnetic field help to improve heat transfer. However, at higher Rayleigh numbers, there is a deterioration in Nu values under the rotary magnetic field over the no magnetic field effect. In the present case, the Rayleigh number increases the mean temperature difference between the hot and cold walls. So, at higher temperature differences, apart from the magnetic force, the thermophoretic force will also play a role. Gravity forces will always be present in the natural convection cavity. The resultant effect of all these forces reduces heat transfer (Nu values) at high Ra values.

If the concentration of nanoparticles increases, then the difference between the rotary magnetic field and no magnetic field will reduce up to $Ra_H = 4 \times 10^8$. More nanoparticles mean more heat carriers. Under the same thermophoretic force, more particles will help in heat transfer from the hot wall to the cold wall. At 0.025% concentration, the heat transfer performance (Nu values) is well above the benchmark paper values when $Ra_H \approx 10^8$. This Rayleigh number can be maintained if the temperature difference is within 10 °C and the bulk fluid temperature (in this case, DM water) is not higher than 35 °C. These ferromagnetic particles are larger (50–100 nm), and their density is higher than that of the alumina nanoparticles (13 nm). So, the nanoparticles will remain in suspension for a longer duration (stability) if external forces like rotary magnetic or thermophoretic forces are present. However, the magnetic effect will be detrimental if the temperature of the bulk fluid is high. The buoyant force and other forces present in the fluid will not be enough for the long suspension of the iron oxide nanoparticles. In comparison with alumina nanoparticles of the same concentration, iron oxide nanoparticles are better heat carriers if stability is maintained.

Now, if more nanoparticles are added to the base fluid, there is still improvement in Nu values up to $Ra_H = 2 \times 10^8$. However, the improvement is not found at higher Ra_H values. At higher temperatures, adding the nanoparticles or employing the rotary magnetic field does not yield any benefit at all if we compare it with the only water case. Because the ferromagnetic nanoparticles will go down more rapidly and settle at the bottom of the cavity at higher temperatures, so, there will be no difference between the base fluid and the nanofluid. Thus, both fluids will produce similar results. The Rayleigh number is comparatively high in the laminar regime. Because the critical Rayleigh number is $\approx 10^9$, laminar flow for natural convection will start transforming into a turbulent regime. Though this cavity size is only 10 cm × 10 cm, we still get such higher Ra values based on the height of the cavity. This also helps the nanoparticles

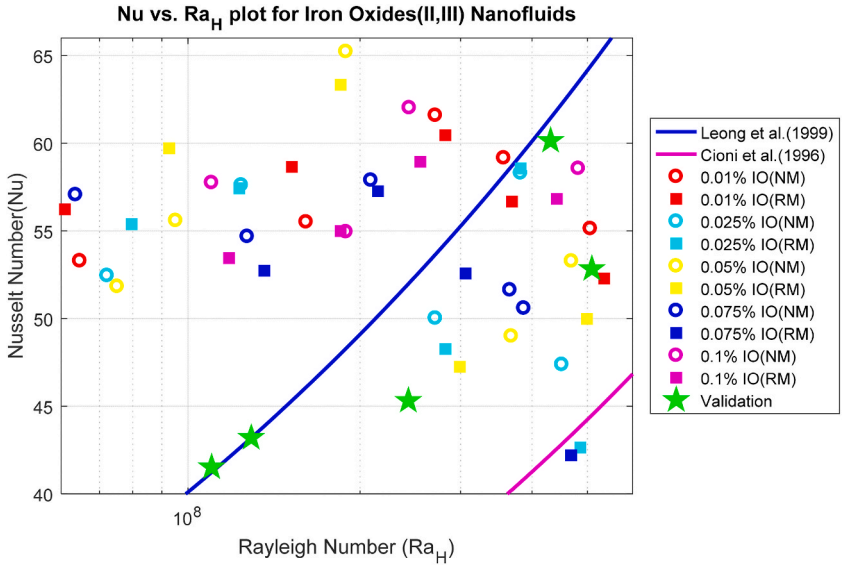

Fig. 11. Nusselt number vs. Rayleigh number plot for iron oxides (II, III) nanofluids.

to mix and flow in the cavity. The benefit of using nanoparticles in the natural convection cavity is found if the Rayleigh number is one order less than the critical Ra_H value.

At 0.075% volume nanofluid concentration, the heat transfer performance trend changes with the Rayleigh numbers. There is a gradual decrease in Nu values with an increase in Ra values under the influence of the rotary magnetic field and also without this field effect. The performance deteriorated further beyond $Ra_H = 3 \times 10^8$ in comparison with the water-only case. Apart from the increased gravity, the decreased buoyant force is also responsible for this performance. In most cases, without the rotary magnetic field effect, heat transfer performance is better. Because the high nanoparticle loading with the magnetic field increases the downward forces. This will be less for non-magnetic cases. Then the nanoparticles or heat carriers will be able to transfer the heat from the hot wall to the cold wall of the cavity. So, after a certain particle concentration, the rotary magnetic field is not required for the improvement of heat transfer. However, nanoparticle introduction into the base fluid has improved heat transfer at a comparatively lower bulk fluid temperature. If we increase the nanoparticle concentrations further, then there will be an improvement for both the rotary magnetic field and also in the absence of the magnetic field. However, at 0.1% by volume, the nanofluid magnetic field is not very effective. Though both cases are much better in terms of heat transformer performance than the water-only case between $Ra_H = 4 \times 10^7$ and $Ra_H = 3 \times 10^8$. These values are much higher than those of Cioni et al. [30]. At this concentration, Nu remains more or less constant over the above Ra_H range. This is contrary to the alumina nanoparticle suspension in DM water; at the same concentration, there is an optimum Ra where Nu is the maximum. So, these ferromagnetic nanoparticles are better at low bulk fluid temperature ranges with a rotary magnetic field. However, without a magnetic field, nanofluid is better in natural convection cavities as long as the temperature of the bulk fluid is not too high and the stability of the solution is ensured. The rotary magnetic field is, in general, more effective for alumina nanoparticles.

In the case of ferromagnetic nanofluids, a large number of outliers are observed at lower Ra values for all ten cases, i.e., Nu has improved concerning the base case (pure water). However, the rotary magnetic field is not recommended for ferromagnetic nanofluids. Because there is a general deterioration in heat transfer in the non-magnetic cases.

6. Conclusion

Iron oxides (II, III) as ferromagnetic and γ-alumina as non-magnetic nanoparticles are used in a 2-L natural convection cavity. As there is no bulk motion in the cavity, the nanoparticle concentration is kept much lower than 1% by volume. Thus, the stability of the nanofluid is maintained. Nanomaterial characterizations are done to confirm the elements (EDS) and their distribution (Color Mapping), the phase identification (XRD), and the sizes (SEM). Five different concentrations of nanofluid solutions are made, and their properties like dynamic viscosity and thermal conductivity are measured. In the presence of a rotary magnetic field and magnetic bead, γ-alumina nanofluid performed the best at $\Phi = 0.1\%$ by volume at about $Ra_H \sim 10^8$. This is true for iron-oxide (II, III) nanofluid as well, except in the absence of a magnetic field. The high Rayleigh number creates local turbulence and mechanical agitation by the bead, enhancing the turbulence. This turbulence improves heat transfer performance. Most of the numerical studies [18] have shown a strange improvement in heat transfer, but experimental results have shown that there is a deterioration in heat transfer. However, in this study, the rotary electromagnetic field enhances the heat transfer for non-magnetic nanofluids in the presence of magnetic bead in the cavity. The current work is focused on only monofluids in the cavity without any surfactants for stabilizing the nanofluid. The cavity is also kept horizontal during all the readings taken during the experiment. In the future, these parameters can be varied, and the

effect on heat transfer will be studied near the critical Rayleigh number.

Funding statement

This is self-funded. There is no external funding for this experimental set-up.

CRediT authorship contribution statement

Debashis Dey: Conceptualization, Investigation, Methodology, Validation, Visualization, Writing – original draft. **Sukanta K. Dash:** Conceptualization, Project administration, Writing – review & editing.

Declaration of competing interest

The authors declare that they have no known competing financial interests or personal relationships that could have appeared to influence the work reported in this paper.

Acknowledgement

Authors are really grateful to Mr. Manas Ranjan Giri and Mr. Bidyadhar Rout (for mechanical components) and Mr. Ambika Prasad Sahoo (for electrical components) for helping us to build this experimental set-up.

Nomenclature

Ra, Ra_H	Rayleigh number
Ra_c	Critical Rayleigh number
Nu_{avg}	Average Nusselt number
h	Convective heat transfer coefficient
V	Volumetric flow rate in LPM
φ	Nanoparticle volume fraction
Cp	Specific heat capacity of the fluid
K_f	Thermal conductivity of the fluid
$T_1..T_4$	Hot wall temperatures
T_H, T_C	Hot and cold wall temperatures
Q_C	Heat removed using the cooling jacket
Gr	Grashof number
Au–Pd	Gold–Palladium
T, G	Tesla, Gauss
μ_{eff}	Effective dynamic viscosity
K_{eff}	Effective thermal conductivity
cP	Centi-Poise
d_p	Nanoparticle diameter size
ρ_{eff}	Effective density
Pr	Prandtl number
H	Height of the cavity
A	Area of the cold or hot wall
$T_5..T_8$	Cold wall temperatures
ΔT	Temperature gain by the water after flowing through the cooling jacket
T_9	Bulk cavity fluid temperature
Re	Reynolds number
Cu	Copper nanoparticles
R^2	Correlation coefficient

References

[1] S.R. Babu, A.S. Chandra, P.R. Babu, Recent developments in synthesis, characterization and boiling heat transfer of nano-fluids – a review, IOP Conf. Ser. Mater. Sci. Eng. 1033 (2021), 012072, https://doi.org/10.1088/1757-899X/1033/1/012072.

[2] R. Sivaraj, S. Banerjee, Transport phenomena of nanofluids in cavities: current trends and applications, Eur. Phys. J. Spec. Top. 231 (2022) 2487–2490, https://doi.org/10.1140/epjs/s11734-022-00635-1.

[3] I.D. Garbadeen, M. Sharifpur, J.M. Slabber, J.P. Meyer, Experimental study on natural convection of MWCNT-water nanofluids in a square enclosure, Int. Commun. Heat Mass Tran. 88 (2017) 1–8, https://doi.org/10.1016/j.icheatmasstransfer.2017.07.019.

[4] Y. Hu, Y. He, C. Qi, B. Jiang, H.I. Schlaberg, Experimental and numerical study of natural convection in a square enclosure filled with nanofluid, Int. J. Heat Mass Tran. 78 (2014) 380–392, https://doi.org/10.1016/j.ijheatmasstransfer.2014.07.001.

[5] M. Sharifpur, S.O. Giwa, K.Y. Lee, H. Ghodsinezhad, J.P. Meyer, Experimental Investigation into natural convection of ZnO-DIW nano-fluids in a square cavity, Heat Tran. Eng. 42 (19-20) (2021) 1675–1687, https://doi.org/10.1080/01457632.2020.1818384.

[6] H. Ghodsinezhad, M. Sharifur, J.P. Meyer, Experimental investigation on cavity flow natural convection of Al_2O_3-water nano-fluids, Int. Commun. Heat Mass Tran. 76 (2016) 316–324, https://doi.org/10.1016/j.icheatmasstransfer.2016.06.005.

[7] A. Rahimi, A. Kasaeipoor, E.H. Malekshah, L. Kolsi, Experimental and numerical study on heat transfer performance of three-dimensional natural convection in an enclosure filled with DWCNTs-water nanofluid, Powder Technol. 322 (2017) 340–352, https://doi.org/10.1016/j.powtec.2017.09.008.

[8] S.Z. Heris, M.B. Pour, O. Mahian, S. Wongwises, A comparative experimental study on the natural convection heat transfer of different metal oxide nano powders suspended in turbine oil inside an inclined cavity, Int. J. Heat Mass Tran. 73 (2014) 231–238, https://doi.org/10.1016/j.ijheatmasstransfer.2014.01.071.

[9] S.U. Ilyas, R. Pendyala, M. Narahari, An experimental study on the natural convection heat transfer in rectangular enclosure using functionalized alumina-thermal oil-based nanofluids, Appl. Therm. Eng. 127 (2017) 765–775, https://doi.org/10.1016/j.applthermaleng.2017.08.088.

[10] K. Kouloulias, A. Sergis, Y. Hardalupas, Sedimentation in nanofluids during a natural convection experiment, Int. J. Heat Mass Tran. 101 (2016) 1193–1203, https://doi.org/10.1016/j.ijheatmasstransfer.2016.05.113.

[11] Y. Chen, Z. Wang, P. Luo, J. Li, D. He, Experimental study of natural convection heat transfer characteristics affected by electrical field with periodically changed direction, Int. J. Therm. Sci. 179 (2022), 107629, https://doi.org/10.1016/j.ijthermalsci.2022.107629.

[12] H. Ghodsinezhad, M. Sharifpur, J.P. Meyer, Experimental investigation on cavity flow natural convection of Al_2O_3–water nanofluids, Int. Commun. Heat Mass Tran. 76 (2016) 316–324, https://doi.org/10.1016/j.icheatmasstransfer.2016.06.005.

[13] E. Khalili, A. Saboonchi, M. Saghafian, Experimental study of nanoparticles distribution in natural convection of Al_2O_3-water nanofluid in a square cavity, Int. J. Therm. Sci. 112 (2017) 82–91, https://doi.org/10.1016/j.ijthermalsci.2016.09.031.

[14] Y. Hu, Y. He, S. Wang, Q. Wang, H.L. Schlaberg, Experimental and numerical investigation on natural convection heat transfer of TiO_2–water nanofluids in a square enclosure, J. Heat Tran. 136 (2) (2014), 022502, https://doi.org/10.1115/1.4025499.

[15] A.B. Solomon, J.V. Rooyen, M. Rencken, M. Sharifpur, J.P. Meyer, Experimental study on the influence of the aspect ratio of square cavity on natural convection heat transfer with Al_2O_3/Water nano-fluids, Int. Commun. Heat Mass Tran. 88 (2017) 254–261, https://doi.org/10.1016/j.icheatmasstransfer.2017.09.007.

[16] E.H. Malekshah, M. Salari, Experimental and numerical investigation of natural convection in a rectangular cuboid filled by two immiscible fluids, Exp. Therm. Fluid Sci. 85 (2017) 388–398, https://doi.org/10.1016/j.expthermflusci.2017.03.023.

[17] Z. Haddad, H.F. Oztop, E. Abu-Nada, A. Mataoui, A review on natural convective heat transfer of nanofluids, Renew. Sustain. Energy Rev. 16 (7) (2012) 5363–5378, https://doi.org/10.1016/j.rser.2012.04.003.

[18] D. Dey, D.S. Sahu, A review on the application of nanofluids, Heat Trans. 50 (2) (2020) 1113–1155, https://doi.org/10.1002/htj.21920.

[19] N. Ahammed, L.G. Asirvatham, S. Wongwises, Thermoelectric cooling of electronic devices with nanofluid in a multiport minichannel heat exchanger, Exp. Therm. Fluid Sci. 74 (2016) 81–90, https://doi.org/10.1016/j.expthermflusci.2015.11.023.

[20] M. Bahiraei, Particle migration in nanofluids: a critical review, Int. J. Therm. Sci. 109 (2016) 90–113, https://doi.org/10.1016/j.ijthermalsci.2016.05.033.

[21] R. Prasher, P. Bhattacharya, P.E. Phelan, Thermal conductivity of nanoscale colloidal solutions (Nanofluids), Phys. Rev. Lett. 94 (2005), 025901, https://doi.org/10.1103/PhysRevLett.94.025901.

[22] S.P. Jang, S.U.S. Choi, Role of Brownian motion in the enhanced thermal conductivity of nanofluids, Appl. Phys. Lett. 84 (2) (2004) 4316–4318, https://doi.org/10.1063/1.1756684.

[23] D. Dey, D.S. Sahu, Experimental study in natural convection cavity using nanofluids, Mater. Today: Proc. 41 (2) (2021) 403–412, https://doi.org/10.1016/j.matpr.2020.09.631.

[24] F. Corvaro, M. Paroncini, An experimental study of natural convection in a differentially heated cavity through a 2D PIV system, Int. J. Heat Mass Tran. 52 (1 – 2) (2009) 355–365, https://doi.org/10.1016/j.ijheatmasstransfer.2008.05.039.

[25] S. Kumar, S.K. Mahapatra, S.S. Das, An experimental and numerical analysis of natural convection in open square enclosure, Heat Tran. Eng. 44 (8) (2022) 1–15, https://doi.org/10.1080/01457632.2022.2086096.

[26] S. Srinivas Rao, Atul Srivastava, Multi view interferometric tomography measurements of convective phenomena in a differentially heated nanofluid layer, Exp. Heat Tran. 1 (2022) 32, https://doi.org/10.1080/08916152.2022.2080302.

[27] D.D. Dixit, A. Pattamatta, Natural convection heat transfer in a cavity filled with electrically conducting nanoparticle suspension in the presence of the magnetic field, Phys. Fluids 31 (2) (2019), 023302, https://doi.org/10.1063/1.5080778.

[28] W.H. Leong, K.G.T. Hollands, A.P. Brunger, Experimental Nusselt numbers for a cubical cavity benchmark problem in natural convection, Int. J. Heat Mass Tran. 42 (11) (1999) 1979–1989, https://doi.org/10.1016/S0017-9310(98)00299-3.

[29] S. Cioni, S. Ciliberto, J. Sommeria, Experimental study of high-Rayleigh number convection in mercury and water, Dynam. Atmos. Oceans 24 (1 – 4) (1996) 117–127, https://doi.org/10.1016/0377-0265(95)00453-X.

[30] N. Putra, W. Roetzel, S.K. Das, Natural convection of nanofluids, Heat Mass Trans. 39 (2003) 775–784, https://doi.org/10.1007/s00231-002-0382-z.

[31] C.H. Li, G.P. Peterson, Experimental studies of natural convection heat transfer of Al_2O_3/DI water nanoparticle suspensions (nano-fluids), Adv. Mech. Eng. 2 (2010), 742739, https://doi.org/10.1155/2010/742.

[32] A. Weppe, F. Moreau, D. Saury, Experimental investigation of a turbulent natural convection flow in a cubic cavity with an inner obstacle partially heated, Int. J. Heat Mass Tran. 194 (2022), 123052, https://doi.org/10.1016/j.ijheatmasstransfer.2022.123052.

[33] D. Dey, A. Kanungo, S.K. Dash, The study of nanofluid properties, nanoparticle characterization, flow visualization, and validation of natural convection cavity setup, Mater. Today: Proc. 74 (4) (2023) 767–773, https://doi.org/10.1016/j.matpr.2022.11.079.

[34] D. Dey, P. Kumar, S. Samantray, A review of nanofluid preparation, stability and thermo-physical properties, Heat Trans. 46 (8) (2017) 1413–1442, https://doi.org/10.1002/htj.21282.